

Inversion of Zeeman polarization for solar magnetic field diagnostics

M. Derouich^{1,2}

¹*Astronomy Department, Faculty of Sciences, King Abdulaziz University, 21589 Jeddah, Saudi Arabia*

²*Sousse University, ESSTHS, Lamine Abbassi street, 4011 H. Sousse, Tunisia*

Abstract

The topic of magnetic field diagnostics with the Zeeman effect is currently vividly discussed. There are some testable inversion codes available to the spectropolarimetry community and their application allowed for a better understanding of the magnetism of the solar atmosphere. In this context, we propose an inversion technique associated with a new numerical code. The inversion procedure is promising and particularly successful for interpreting the Stokes profiles in quick and sufficiently precise way. In our inversion, we fit a part of each Stokes profile around a target wavelength, and then determine the magnetic field as a function of the wavelength which is equivalent to get the magnetic field as a function of the height of line formation.

To test the performance of the new numerical code, we employed “hare and hound” approach by comparing an exact solution (called input) with the solution obtained by the code (called output). The precision of the code is also checked by comparing our results to the ones obtained with the HAO MERLIN code. The inversion code has been applied to synthetic Stokes profiles of the Na D₁ line available in the literature. We investigated the limitations in recovering the input field in case of noisy data. As an application, we applied our inversion code to the polarization profiles of the Fe I λ 6302.5 Å observed at IRSOL in Locarno.

Email address: derouichmoncef@gmail.com (M. Derouich^{1,2})

Keywords: Polarization– Magnetic fields – Sun: atmosphere – Line: formation – Line: profiles

1. Introduction

In the quiet Sun, where the magnetic field is weak, the Zeeman splitting can be smaller than the Doppler width of the spectral lines; in these conditions the Zeeman effect cannot be observed and one must use the Hanle effect technique to obtain the solar magnetic field (e.g. Stenflo 1982; Landi Degl’Innocenti 1983; Sahal-Br  chot et al 1986; Trujillo Bueno et al. 2004; Derouich et al. 2006; Faurobert et al. 2009; Derouich et al. 2010). However, in the active regions where the magnetic field is sufficiently strong, the Zeeman effect produces a measurable splitting of the atomic levels and a subsequent polarization of the emitted light (e.g. Harvey et al. 1972; Jefferies et al. 1989; Socas-Navarro et al. 2000; Asensio Ramos et al. 2012).

Rigorous interpretation of the Zeeman effect on the spectral polarization can be a crucial source of information about the Sun’s magnetic field. It is necessary to apply suitable theoretical and numerical methods to extract the physical information from spectro-polarimetric solar observations. To this aim, from the beginning of the 70’s of the 20th century, vigorous theoretical and numerical efforts have been made to develop non-linear inversion codes that are able to reliably derive information about the magnetic properties of the solar plasma. The present work is a new contribution to these efforts. Our aim is to illustrate a new inversion procedure in order to search for new possibilities to determine the structure and distribution of the solar magnetic field. The inversion technique uses the equations established by Landi Degl’Innocenti and Landi Degl’Innocenti (1972), and later by Jefferies et al. (1989) and Stenflo (1994).

In this work, we focus on the accuracy of the fitting algorithms of the Stokes profiles to ensure maximum performance of the inversion technique. In fact, for the familiar Zeeman effect, the responsible physical mechanisms are typically

already well understood¹. Therefore, the advances in the inversions codes, which are based on the Zeeman effect, should be mainly concentrated on how to fit the Stokes profiles in order to deduce the magnetic field. It is the intention of this paper to find out the best fitting strategy. Careful fitting of the Stokes profiles allows to reduce significantly the error bar on the determination of the magnetic field. This work proposed useful methods to achieve a proper fit of the Q, U, V, and I-profiles.

In order to validate our numerical code, through a controlled and pragmatic strategy, we adopt “hare & hound” approach consisting of the following steps:

(1) We make use of synthetic Stokes profiles of the Na I λ 5896 Å line available in the literature (Uitenbroek (2001, 2003, 2011), Leka et al. 2012). The magnetic maps which served to generate these Stokes profiles, with the aid of 3D NLTE radiative transfer models, are also available and are called *input*.

(2) We analyze the synthetic Stokes profiles using our inversion code, and attempt to retrieve the magnetic maps (called *output*)

(3) We compare the exact solution (input) with the solution provided by the inversion code (output).

(4) We analyze the dependence of the results on the signal-to-noise ratio. Different levels of expected noise are then simulated to evaluate their impact on the precision of our results. This allows us to determine the needed polarimetric sensitivity and estimate the error bars in the determination of the solar magnetic field.

In addition, the precision of the code is also checked by comparing our results to the ones obtained with the HAO MERLIN code. The comparison is based on the level 1 and level 2 data available online at the Community Spectropolarimetric Analysis Center.² Finally, using our numerical code we interpret Fe I λ 6302.5 Å observed at IRSOL in Locarno.

¹This is in contrast of the Hanle effect for which a variety of less familiar physical mechanisms are still not well understood.

²CSAC; <http://www.csac.hao.ucar.edu/>

2. Inversion method

The inversion formalism is based on the equations obtained by Landi Degl’Innocenti and Landi Degl’Innocenti (1972), and later by Jefferies et al. (1989) and Stenflo (1994). According to these equations, the Stokes parameters are related in a simple way to the magnetic field vector under the weak field approximation. The domain of validity of these equations was reviewed and presented in Table 9.1 of a monograph by Landi Degl’Innocenti & Landolfi (2004). The inversion code allows us to deduce the magnetic field by fitting theoretical profiles to the observed ones.

2.1. Fitting of the I -profiles

We adopted, the well known Voigt line shape to fit the intensity profiles. Voigt function depends on five parameters: the continuum of the profile, the line strength, the damping parameter, the Doppler width, and the value of the line center. The fitting consists of the determination of these five parameters. Our fitting strategy is divided into three steps. The first step consists of obtaining a first guess. In this first step we use an uniform weighting to all points in the profile. Using the results of the initial analysis, as a second step, we change the weights of some points in the sense of improving the determination of the continuum intensity, the line strength and the line center. The inversion method developed in this work permits the magnetic field determination in a given target wavelength $\delta\lambda_B$. Therefore, in the third step only a part of the intensity profile surrounding $\delta\lambda_B$ is well fitted. With this aim, the choice of weighting is done in such a manner as to obtain the best Voigt-fitting around the target wavelengths where the magnetic field is determined. The third step permits especially the determination of the Doppler width and the Doppler damping. Figure 1 represents an example of the fitting of an intensity profile where the second and the third steps are illustrated.

Now one uses the results of the fitting of the I -profile to obtain the Voigt function $H(a, v)$ and the Faraday-Voigt function $F(a, v)$; $H(a, v)$ is associated

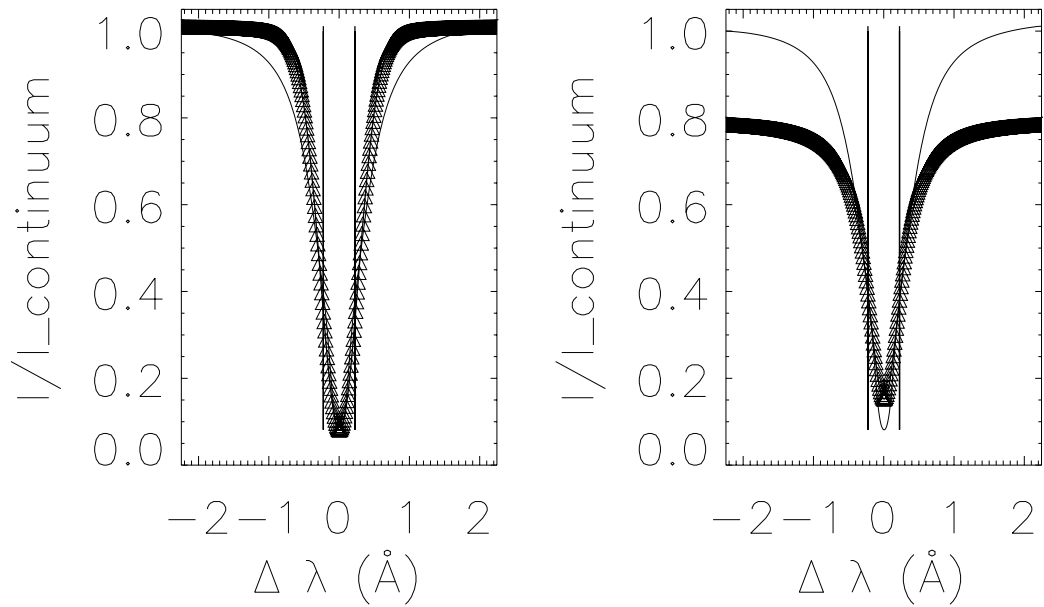


Figure 1: A plot representing a Voigt function fit of the intensity profile of an umbra pixel. This fit is performed as follows. The open triangles (Δ) represent the theoretical profile resulted from the fitting procedure. Left: the weighting is taken in a manner to improve the determination of the continuum intensity, the line strength and the line center. The vertical line represents the place of the target wavelength $\delta\lambda_B = 0.224520 \text{ \AA}$. Right: the weighting is changed in a way to obtain the best Voigt-fitting around the target wavelengths where the magnetic field will be determined.

to the absorption coefficient which is proportional to the imaginary part of the complex refractive index and $F(a, v)$ is associated to the real part of the complex refractive index. Note that $F(a, v)$ indicates the measurable consequences of the changes of the phase velocity of the wave in the atmosphere. Here a is the Voigt parameter and $v = \delta\lambda_B/\delta\lambda_D$, where the target wavelength $\delta\lambda_B$ represents the shift in wavelengths due to the Zeeman effect of the magnetic field and $\delta\lambda_D$ is the Doppler width of the intensity profile. In addition, one can determine the values of $H'(a, v) = \frac{\partial H}{\partial v}$, $H''(a, v) = \frac{\partial^2 H}{\partial v^2}$ and $\frac{\partial I}{\partial \lambda}$ which gives the variation of the intensity I (in arbitrary units) for a small variation $d\lambda$ (in Angström) along the I -profile. Considering that S designates the line strength, in the Voigt fitting case, one can show that,

$$\frac{\partial I}{\partial \lambda} = -2S \times [2 - a - F(a, v) - v - H(a, v)]/\delta\lambda_D \quad (1)$$

2.2. Fitting of the polarization profiles

Once the intensity profile is well-fitted, we fit the Stokes parameters Q , U , and V . The fitting of Stokes Q , U and V is obtained with the Singular Value DeComposition (SVDC) and Singular Value SOLve (SVSOL) routines. The SVDC expands the original data that we are trying to fit in a 4-dimensions basis. We checked other possible dimensions and we found that a 4-dimensions basis is more appropriate. After that, the SVSOL uses the results of the expansion generated by SVDC in order to fit the polarization profiles, i.e. obtaining the solution which corresponds to the minimization of the χ^2 . An example of the result of the fitting of the polarization profiles is given in the Figure 2.

It is worth noticing that the fitting of the Stokes parameters is performed after convolution of the original spectra. The convolution is typically needed to smooth the profile and to decrease the effect of the noise. Generally, one can perform the convolution with a rectangle or kernel functions, or with an instrumental profile.

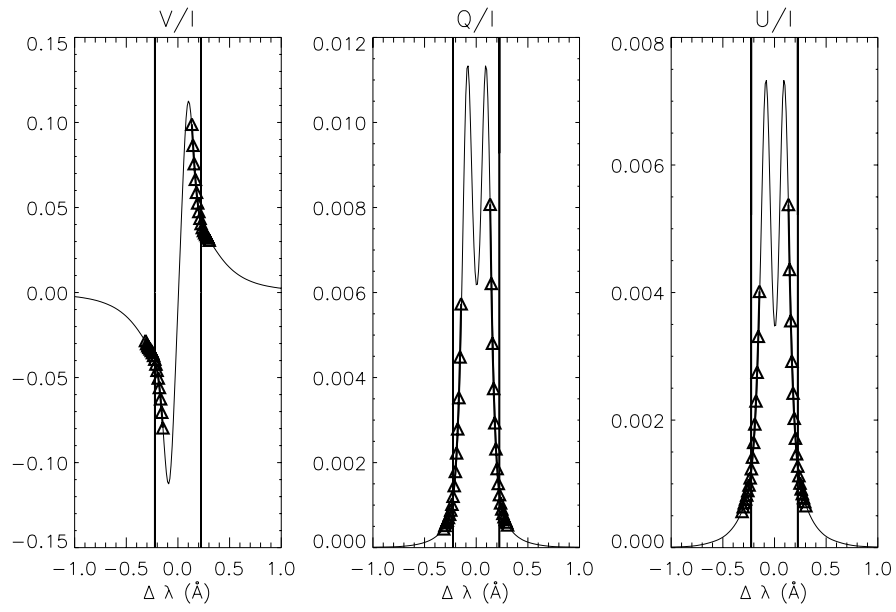


Figure 2: Fit of Q, U and V profiles of an umbra pixel: SVDC and SVSOL methods applied to Non-LTE synthetic Na I λ 5896 Å line. The open triangles (Δ) represent the theoretical profile resulted from the fitting procedure. The vertical lines represent the place of the target wavelength $\delta\lambda_B = 0.224520$ Å.

2.3. From the best fit profiles to the magnetic vector

The magnetic vector can be determined in the Cartesian coordinates (B_x, B_y, B_z) or in the spherical coordinates (B, θ, δ) . The representation of these coordinates is illustrated in the Figure 3. Geometric relations between the Cartesian components of the magnetic field (B_x, B_y, B_z) and its spherical coordinates (B, θ, δ) are:

$$\begin{aligned} B_x &= B \sin \delta \cos \theta \\ B_y &= B \sin \delta \sin \theta \\ B_z &= B \cos \delta \end{aligned} \quad (2)$$

The longitudinal part of the magnetic field is $\vec{B}_{LOS} = \vec{B}_z$ and the transverse part is $\vec{B}_{Trans} = \vec{B}_x + \vec{B}_y$. The angles δ and θ satisfy the following equations:

$$\begin{aligned} \theta &= \tan^{-1}\left(\frac{B_y}{B_x}\right) \\ -\pi &\leq \theta \leq \pi \end{aligned} \quad (3)$$

and,

$$\begin{aligned} \delta &= \cos^{-1}\left(\frac{B_z}{B}\right) \\ -\frac{\pi}{2} &\leq \delta \leq \frac{\pi}{2} \end{aligned} \quad (4)$$

After solving the radiative transfer equations, one could demonstrate that (e.g. Landi Degl'Innocenti and Landi Degl'Innocenti (1972) and Jefferies et al. (1989)):

$$B_{LOS}(Gauss) = \frac{-2.142 \times 10^{12}}{g \times \lambda_0^2} \times \frac{V}{\left(\frac{\partial I}{\partial \lambda}\right)}, \quad (5)$$

and the transverse magnetic field:

$$\begin{aligned} |B_{Trans}(Gauss)| &= 2 \times \frac{2.142 \times 10^{12}}{g \times \lambda_0^2} \\ &\times \sqrt{\frac{|H'(a, v)|}{v \times |H''(a, v)|} \times \sqrt{(Q^2 + U^2)} \times \left|\frac{\delta \lambda_B}{\left(\frac{\partial I}{\partial \lambda}\right)}\right|} \end{aligned} \quad (6)$$

and the inclination:

$$\theta = \frac{1}{2} \tan^{-1}\left(\frac{U}{Q}\right) \quad (7)$$

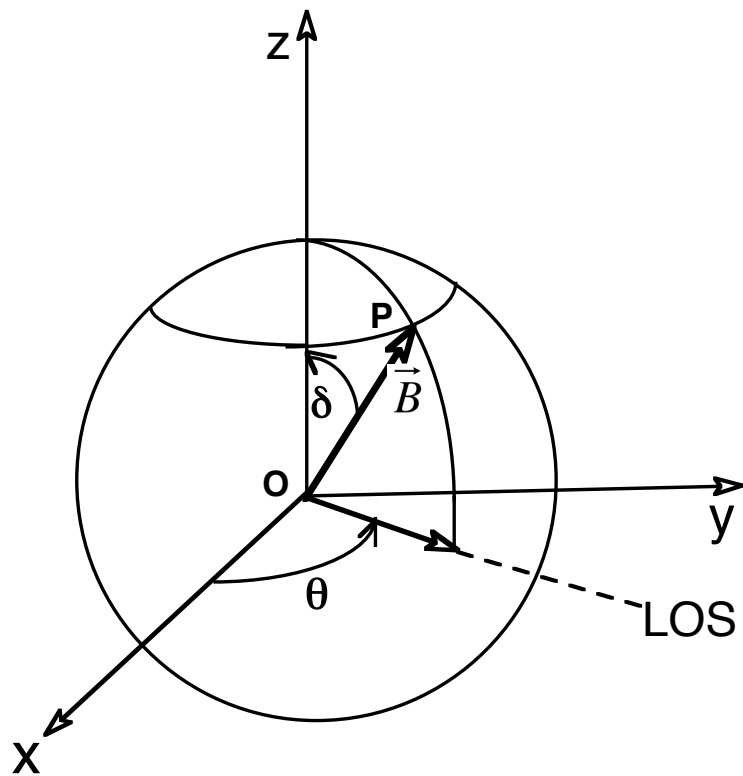


Figure 3: An illustration of the Cartesian and spherical coordinates of the magnetic field.

Equations (4, 5, 6, 7) are used through this paper to determine the magnetic maps.

Note that the equation (6) gives only the absolute value of B_{Trans} . It means that the fundamental ambiguity is not solved. Two field vectors that are symmetrical with respect to the line-of-sight (LOS) have the same polarimetric signature.

3. Results of the inversion of the synthetic Stokes profiles of the Na I λ 5896 Å line

Our objective is to determine the values of the Stokes spectra at the target wavelengths $\delta\lambda_B$ and to introduce them in the Equations 4–7 to obtain the magnetic vector. We do not fit the whole profile but we only fit the part of the profile defined by

$$\delta\lambda = \delta\lambda_B \pm \delta\lambda_{TOL} \quad (8)$$

$\delta\lambda$ is the shift in wavelengths from the line center and the $\delta\lambda_{TOL}$ is called tolerance, which is arbitrary. In principle the value of the magnetic field vector does not depend on the choice of the tolerance value. However, it should be noticed that for small values of tolerance the magnetic field jumps very quickly which means that for small values of tolerance the inversion method is not stable numerically. Typically, $30 \text{ mA} \leq \delta\lambda_{TOL} \leq 90 \text{ mA}$.

To test the performance of our fitting method we employ “hare & hound” approaches consisting of comparison between the exact solution (input) and the solution provided by the inversion method (output). Figure 4 represents the theoretical perfect correspondence (output=input) and the result of the fit (output vs input). It is to be mentioned here that the NLTE approach and the atomic model used to generate the Stokes vector (Uitenbroek (2001, 2003, 2011), Leka et al. 2012) is different from the NLTE approach and the atomic model adopted in our inversion method, which would make some inevitable differences between input and output magnetic fields even in zero-noise case.

A noise level = 10^{-4} is added to a map of 142×128 pixels. Each pixel contains the synthetic Stokes profiles. We invert the data obtained for an observing angle $\mu=1$ where, for the synthetic Stokes profiles studied here, the circular polarization is clearly larger than the linear polarization (see Leka et al. 2012). As a result of the inversion, we find that the averaged relative error in the case of the longitudinal magnetic field is 12%. For the transverse component, we found that the relative error is 35%. In the case of the inclination angle, the averaged relative error is 30%. The relative error is smaller in the case of the longitudinal magnetic field due to its dependence on the circular polarization V which is sufficiently large. On the contrary, the transverse field depends on the linear polarization which is small and its determination is very sensitive to the noise. The inclination depends on both the linear and the circular polarizations.

Let us mention that the synthetic Stokes profiles contain pixels in quiet Sun, plage, umbra and penumbra. Thus, one should take into account that, for example, magnetic fields in quiet Sun pixels with absolute values lower than 10 Gauss are not able to reproduce measurable Zeeman effect and thus are not easily recovered in the output. This could explain why the averaged error seems to be rather large especially in the case of the transverse field and the inclination.

In the case of the azimuth, we found difficulties in comparing the input with the output. In order to understand the source of these difficulties, we decided to compare the azimuth angle using the input magnetic field via the equation $\theta_1 = \tan^{-1}(\frac{B_y}{B_x})$ to the azimuth angle that one obtains from the equation $\theta_2 = \frac{1}{2} \tan^{-1}(\frac{U}{Q})$. Interestingly, U and Q are the synthetic NLTE emergent Stokes parameters generated from the input magnetic field $\vec{B}(B_x, B_y, B_z)$, i.e. θ_1 and θ_2 are inferred from the input. Thus, in principle, θ_1 and θ_2 must be similar. However, we found them quite different. The possible explanation of this discrepancy is that the components B_x and B_y are determined in a reference different from the reference in which Stokes parameters were calculated. Consequently, in the case of the azimuth, we could not compare correctly the input with the output.

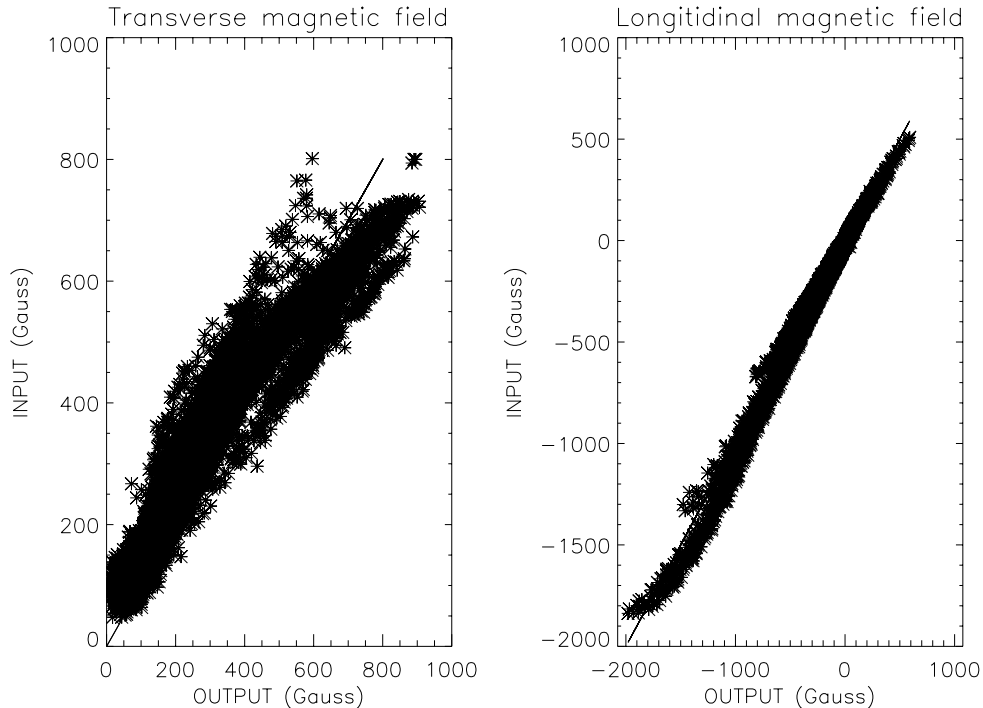


Figure 4: A plot representing the output and the input of the longitudinal and transverse magnetic fields. A noise level $= 10^{-4}$ is added to the theoretical Stokes profiles used in the inversion. The output is showed with stars *.

Note that only the Stokes parameters U and Q are defined with respect to a given reference direction. When the reference direction changes, Q and U tend to change into each other. The Stokes V , the intensity I and the complete linear polarization $\sqrt{U^2 + Q^2}$ are invariant under rotation of the reference direction.

4. Effect of the noise

In order to evaluate the effect of the noise, we investigate the reliability of the fitting accuracy in case of noisy Stokes spectra by computing the standard deviation σ . Furthermore, we compare the magnetic field obtained in a zero noise case to the one obtained in a noisy case.

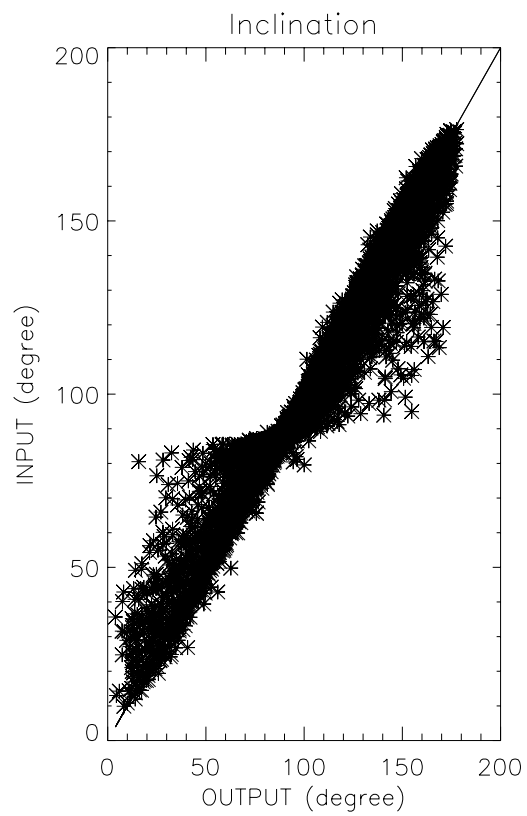


Figure 5: A plot representing the output and the input of the Inclination. A noise level = 10^{-4} is added to the theoretical Stokes profiles used in the inversion. The output is showed with stars *.

σ_V	0.00376968	0.00198307	0.000884621	0.000640550	0.000548571	0.000527108	0.000514566
σ_U	0.00404129	0.00193955	0.000788354	0.000412921	0.000258710	0.000213259	0.000175086
σ_Q	0.00395388	0.00202286	0.000896636	0.000575089	0.000443220	0.000431046	0.000412398
noise	0.005	0.0025	0.001	0.0005	0.0001	5×10^{-5}	0.00

Table 1: σ values resulted from the SVDC and SVSOL fitting.

4.1. Standard deviation σ for polarization profiles fitting

In our work we use numerically-generated Stokes profiles from a known magnetic model (Uitenbroek (2001, 2003, 2011), Leka et al. 2012). These profiles are artificially polluted with noise. At each noise level, one added poisson-distributed noise to an umbra pixel and 1000 noise realizations of the data were generated. We compute the standard deviation σ which is given by :

$$\sigma = \sqrt{\frac{\sum (x_i - x_{exact})^2}{N - 1}} \quad (9)$$

where, i is an index to indicate a given realization and N is the total number of realizations ($N=1000$). The symbol x_i represents a Stokes parameter Q/I , U/I , or V/I of a given realization and x_{exact} is the exact value of the Stokes parameter at the umbra pixel. Our fit via the SVDC and SVSOL procedures was performed around a target wavelength $\delta\lambda_B=0.134712 \text{ \AA}$ and the tolerance $\delta\lambda_{TOL}=45 \text{ m\AA}$. Table 1 shows low standard deviations σ_V , σ_U and σ_Q which means that the Stokes profiles are well fitted and the results must be reliable.

4.2. Magnetic field in a zero noise case vs noisy case

As we mentioned previously, even in zero noise case, some inevitable differences between input and output magnetic fields occur. In order to exclude the effects of other factors and to evaluate exclusively the effect of the noise, we compare a noisy output to a zero noise output. Therefore, we compare the magnetic field derived in the case where the effect of the noise is added to the one derived in the zero noise case. We start by adding a low noise level= 5×10^{-5} . Figure 6 shows the comparison between the exact solution corresponding to the equation of a straight line passing through the origin and the solution affected

by the noise. It is clear from the Figure 6 that the effect of the noise is small and the accuracy for the determination of the magnetic field is good. This is especially the case for the longitudinal component where the difference between the noisy and non-noisy cases is less than 5%. In the case of the transverse magnetic field, the difference can reach up to 25%.

Let us now calculate the error percentage on the magnetic field determination in the case of a noise level= 2.5×10^{-3} . Figure 7 represents, with a solid line, the theoretical exact solution corresponding to the equation $y = x$ in the Cartesian coordinates. Moreover, in the same figure, the open triangles represent the magnetic field obtained in the noisy case as a function of the magnetic field derived in the zero noise case. The difference between the noisy and non-noisy cases is less than 7 % in the case of the longitudinal magnetic field, however, it can be up to 75 % in the case of the transverse magnetic field. Thus, for many pixels the noise is so important that it is impossible to derive the transverse magnetic field from the observation of the linear polarization in the sodium line. It is worth mentioning that the modest effective Landé g-factor of the Na I λ 5896 Å line ($g = 1.33$) contributes to an expected weak linear polarization signal.

As a conclusion, one should consider that for a noise level $> 10^{-3}$, it is difficult to correctly interpret the Na I linear polarization in terms of transverse magnetic field. The situation must be better for the Fe I line λ 6302.5 Å owing to its high sensitivity to magnetic fields. In fact, its Landé factor ($g = 2.5$) is almost two times larger than the Landé factor of the Na I line. In any case, by inverting the synthesized Stokes profiles of the Na I line, our aim was only to test our inversion method, and not to know anything about the solar magnetic field.

As an application, our numerical code is applied to the Fe I λ 6302.5 Å line which is widely used for solar magnetometry.

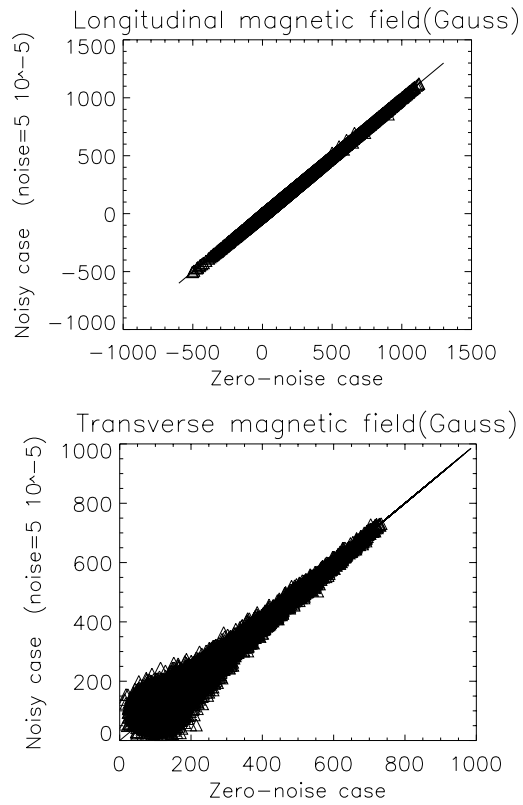


Figure 6: A plot representing the effect of a noise level= 5×10^{-5} . The solid line shows the theoretical exact solution corresponding to the equation $y = x$ in the Cartesian coordinates. The open triangles (Δ) represent the magnetic field obtained in the noisy case as a function of the magnetic field derived in the zero noise case.

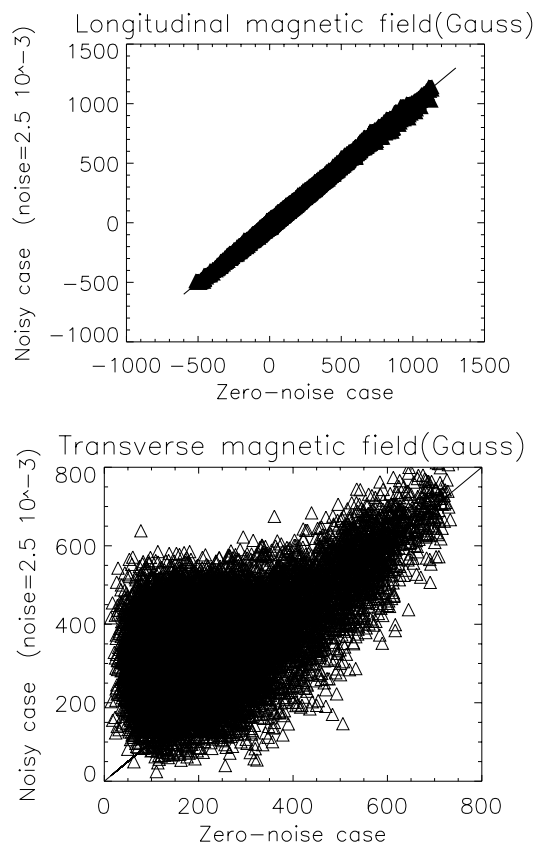


Figure 7: The same as Figure 6 but the noise level= 2.5×10^{-3} .

5. MERLIN inversion code vs. our numerical code

We use full spectra data of Hinode Solar Optical Telescope-Spectropolarimeter (SOT-SP) obtained for the Fe 6302.5 Å line (Kosugi et al. 2007; Tsuneta et al. 2008; Lites et al. 2013). Stokes profiles (level 1) and level 2 outputs from inversions using the HAO MERLIN inversion code developed under the Community Spectropolarimetric Analysis Center are available online.

This allows us to compare our code with the MERLIN code. It is worthy noticed that MERLIN inversions are performed at every pixel regardless of polarization profile, and the inversion code caps the field strength values at 5000 Gauss, so it will not give values larger than that. If a pixel reaches a value of 5000 Gauss, then one can assume that the code has not converged properly for that pixel. For other quiet Sun pixels, the magnetic field is about 3000 or 4000 Gauss but we verified that the corresponding polarization signals are weak which means that MERLIN gives clearly incorrect results for that pixels. Before the comparison, I removed the polarization profiles giving spurious and unphysical results.

Level 2 file chosen here is '20160903__074908.fits' which corresponds to the inversion of 1139 profiles of polarization presented in level 1 data; i.e. the slit of the SP instrument scanned the solar surface in 1139 steps to construct a 2D image of the solar surface. The level 1 data are calibrated profiles of polarization containing 3D data (spectral x spatial x 4 Stokes parameters) ready for scientific analysis. For direct comparison, I inverted the same level 1 profiles and confronted our results to the MERLIN's results.

The results are encouraging and give us the conviction that the code provides sufficiently precise output although that it is based on rather simple assumptions. Figure 8 shows, with a solid line, the theoretical exact solution corresponding to the equation of a straight line passing through the origin and the result of the comparison between the solution corresponding to our results and the solution obtained by MERLIN.

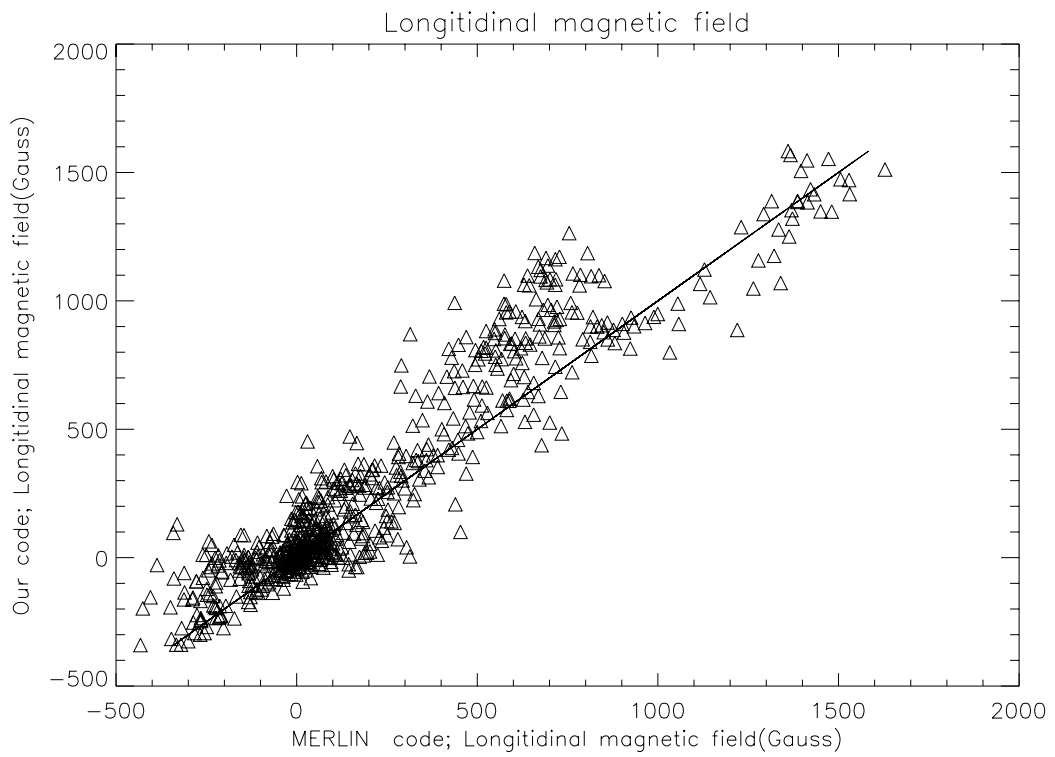


Figure 8: MERLIN inversion code VS our code.

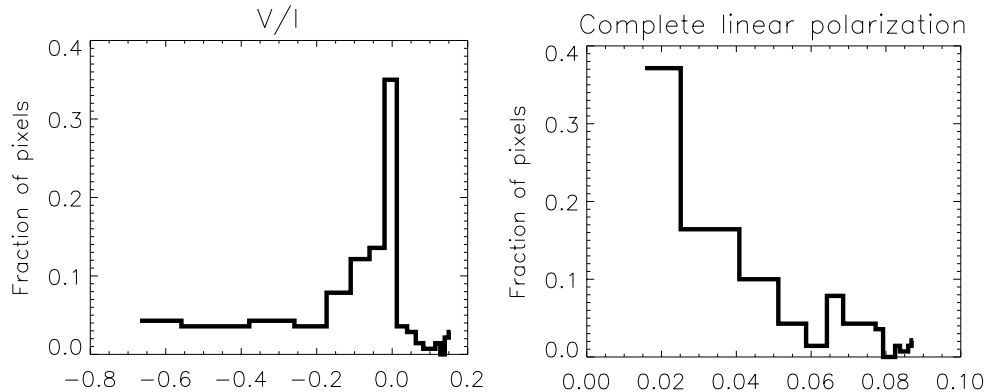


Figure 9: Fraction of pixels at each range of values of the circular polarization V/I and complete linear polarization $\sqrt{Q^2 + U^2}/I$ which are directly related to the longitudinal and transverse magnetic field, respectively.

6. Application: inversion of the observations of the polarization profiles of the Fe I λ 6302.5 Å line

6.1. Observations

The observations of the polarization profiles of the Fe I λ 6302.5 Å line has been kindly communicated to us by Dr. Michele Bianda (IRSOL). The observations were performed on April 10, 2016, at IRSOL in Locarno using the 45 cm aperture Gegory Coudé telescope, the 10 m focal length Czerny-Turner spectrograph (grating 180 mm x 360 mm, 316 lines / mm), and ZIMPOL (Ramelli et al. 2010).

The observed sunspot was AR2529 located near the East limb. The spectrograph slit, oriented parallel to the solar polar limbs, or perpendicular to the solar rotation axis, was crossing the sunspot. The slit-width of 60μ corresponds on the solar image to 0.5 arcsec.

The high modulation rate of 1 kHz delivered by the FLC modulator of ZIMPOL permits to overcome spurious polarization signatures originated by seeing effects. The FLC modulator is designed following the Gisler method (Gisler 2005).

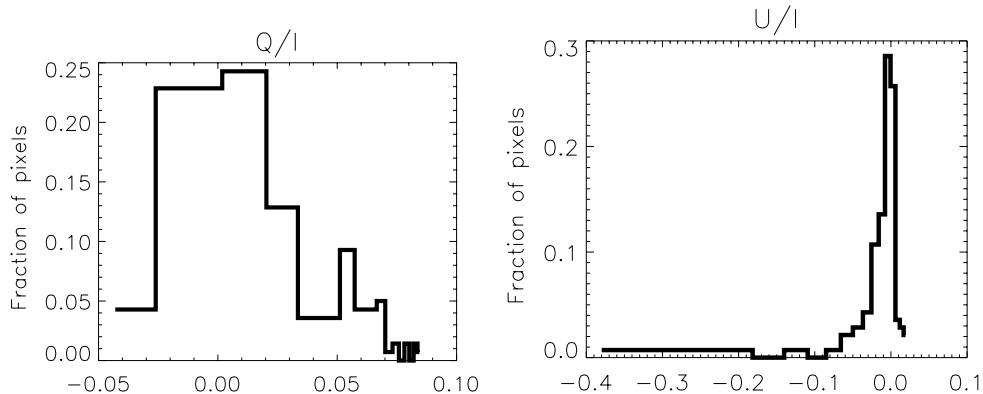


Figure 10: Fraction of pixels at each range of values of the Stokes parameters Q/I and U/I .

Reduced data is the combination of 4 CCD recordings of 0.2 s exposure each (see Ramelli et al. 2010 for details). That is a short time compared to the usual ZIMPOL observations intended to measure scattering polarization signatures where precision in the order down to 10^{-5} is required. In the observation reported here a noise in the order of 2×10^{-3} is reached, but the short exposure reduces the image quality degradation originated by the seeing. Consequently, as one is working with large signatures, that is an advantage.

The observing angle is $\sim 50^\circ$. For this observation angle, the complete linear polarization $\sqrt{Q^2 + U^2}/I$ reaches the values larger than the circular polarization V/I . The transverse component of the magnetic field is expected to be larger than the longitudinal one. It is worth mentioning that if the angle of observation is changed, the observed Stokes profiles will be changed. Thus, the components \vec{B}_{Trans} and \vec{B}_{LOS} will be changed. However, the magnetic field vector $\vec{B} = \vec{B}_{Trans} + \vec{B}_{LOS}$ does not depend on the angle of observation. The inversion provides a unique output (i.e. unique magnetic field vector).

We notice in the Figures 9 and 10 that about 30% of the observed pixels have a small polarization. That will directly affect the values of the magnetic field.

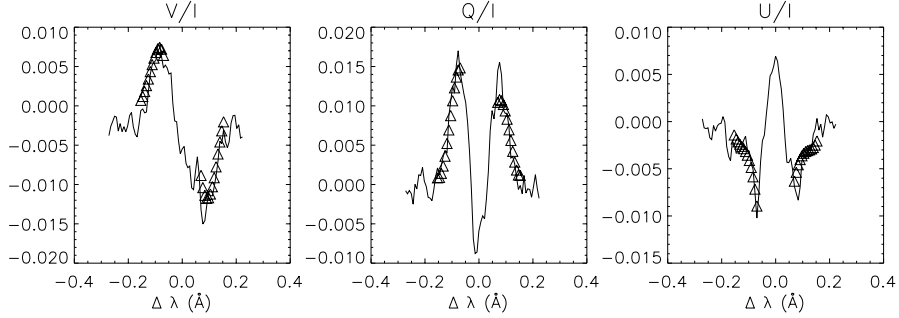


Figure 11: Example of the fitting of the observations using SVDC and SVSOL methods for a Q, U and V parameters. The tolerance adopted is $\delta\lambda_{TOL}=0.045$ Å and the place of the target wavelength $\delta\lambda_B=0.109863$ Å. The open triangles (Δ) represent the theoretical profile resulted from the fitting procedure.

6.2. Determination of the magnetic field vector

We started by fitting the observed intensity and polarization profiles. An example of the results of the fit is presented in the Figure 11. Then we computed the magnetic field vector inferred from the observations. The results are presented in histograms that count the fraction of pixels in each range of values. The majority of the observed pixels have a small value of the magnetic field. There is a clear correlation between the values of the magnetic fields presented in the Figure 12 and those of the polarization in the Figures 9 and 10.

Figure 13 indicates that between ~ 10 % and 20 % of pixels have a magnetic field inclined of about 80° to 100° from the horizontal. The azimuth angle is mainly around 10° .

7. Final remark: combining the bisector method with our inversion method

The bisector method tells us that:

$$B_{LOS}(Gauss) = \frac{1.071 \times 10^{12}}{g \times \lambda_0^2} \times (\lambda_+ - \lambda_-) \quad (10)$$

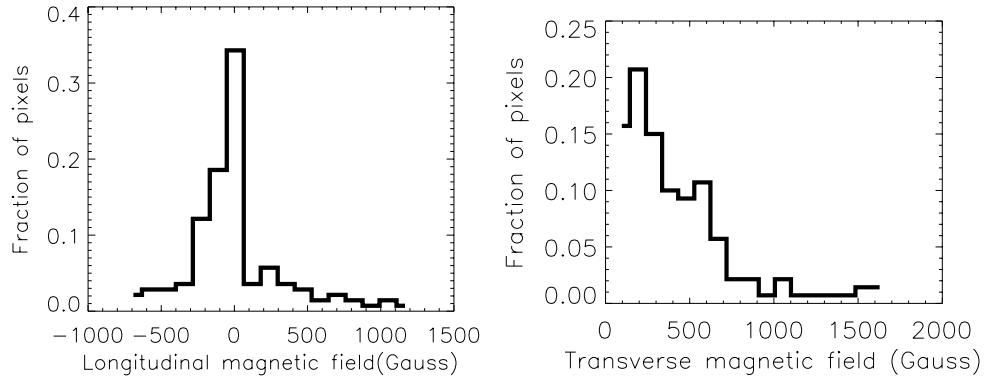


Figure 12: Fraction of pixels at each range of values of the transverse and the longitudinal components of the magnetic field.

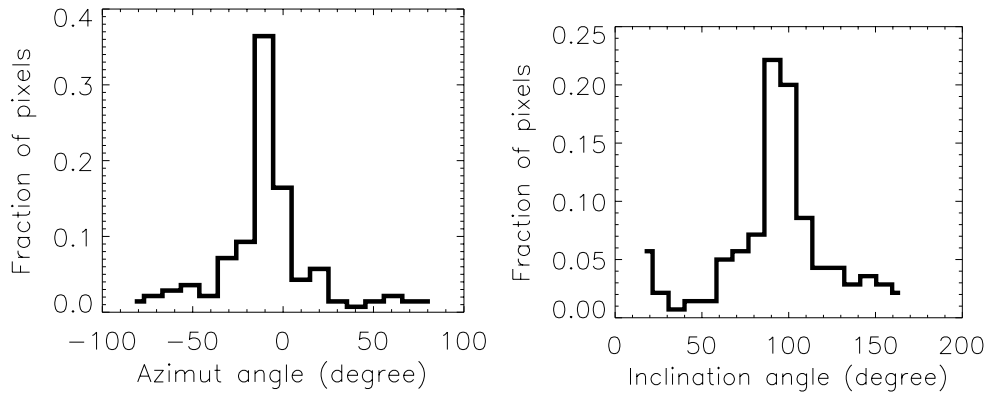


Figure 13: Fraction of pixels at each range of values of the azimuth and the inclination angles.

where λ_+ is the central wavelength or bisector location of $I + V$ profiles and λ_- is the bisector location of $I - V$ profiles (Rayrole 1967, Semel 1967).

By comparing B_{LOS} of the Equation 5 and the Bisector expression of B_{LOS} given by Equation 10, one concludes that both are exactly the same if:

$$\frac{-2 \times V}{\left(\frac{\partial I}{\partial \lambda}\right)} = (\lambda_+ - \lambda_-) \quad (11)$$

The value of $\frac{\partial I}{\partial \lambda}$ can be determined using the bisector method and then introduced in the Equation 6. Thus the bisector method could be used to obtain the LOS magnetic field but also could contribute in the determination of the transverse magnetic field. It is worth noticing that the bisector method is valid even for strong magnetic fields.

8. Conclusions

Zeeman polarization in the solar lines can be a crucial source of information about photospheric and chromospheric magnetic fields.

The main concern of our work was to develop a new inversion code based on Zeeman effect and to evaluate its accuracy for future applications. We showed that our code gives results with a satisfactory precision. For a given input magnetic field configuration, one can synthesize Stokes profiles emergent from solar atmosphere for any value of the observation angle μ . We inverted the data obtained for $\mu=1$. Using the method presented in our work, it is possible to determine the variation of the magnetic field vs the target wavelength $\delta\lambda_B$ which is equivalent to the variation of the magnetic field with the height in the atmosphere. The choice of the tolerance follows the best compromise that we found between stability of the inversion method and obtaining the magnetic variation as a function of the wavelengths. As an additional test to the precision of the inversion code, we used the level 1 and level 2 data available online at the Community Spectro-polarimetric Analysis Center to compare our results with the results obtained with the HAO MERLIN inversion code.

Finally, as an application, we inverted real observations that were performed on April 10, 2016, at IRSOL in Locarno.

Acknowledgments

I am greatly indebted to Dr. Michele Bianda (IRSOL, Switzerland) for communicating to me unpublished observations and I would like to thank Dr. Graham Barnes and Dr. K.D. Leka for helpful discussions during my stay in CoRA (USA). HINODE is a Japanese mission developed and launched by ISAS/JAXA, with NAOJ as domestic partner and NASA and STFC (UK) as international partners. It is operated by these agencies in cooperation with ESA and NSC (Norway). Hinode SOT/SP Inversions were conducted at NCAR under the framework of the Community Spectro-polarimetric Analysis Center (CSAC; <http://www.csac.hao.ucar.edu>).

References

- Asensio Ramos A., Manso Sainz R., Martínez González M. J., Viticchié B., Orozco Suárez D., Socas-Navarro H., 2012, *ApJ*, 748, 14
- Derouich M., Bommier V., Malherbe J.M., Landi Degl’Innocenti E., 2006, *A&A*, 457, 1047
- Derouich M., Auchère F., Vial J. C., Zhang M., 2010, *A&A*, 511, 7
- Faurobert M., Derouich M.; Bommier V., Arnaud J., 2009, *A&A*, 493, 201
- Gisler D., 2005, Instrumentierung für hochpräzise Vektorpolarimetrie in der Astronomie, PhD thesis, ETH-Zurich, No. 16110
- Harvey J., Livingston W., Slaughter C., 1972, In *Line Formation in the Presence of Magnetic Fields*, High Altitude Observatory, NCAR, Boulder, Colorado, p. 227.
- Hauge, P.S.: 1976, in W.L. Hyde and R.M.A. Azzam (eds.), *Polarized Light*, Proc.
- Jefferies J.T., Lites B.W., Skumanich A., 1989, *ApJ*, 343, 920
- Kosugi, T., Matsuzaki, K., Sakao, T., et al. 2007, *Sol. Phys.*, 243, 3
- Landi Degl’Innocenti E., 1983, *Solar Phys.*, 85, 33
- Landi Degl’Innocenti E., Landi Degl’Innocenti M., 1972, *Solar Phys.*, 27, 319 (see erratum in *Solar Phys.* 29, 528).
- Landi Degl’Innocenti E., Landolfi M., 2004, *Polarization in Spectral Lines*

(Dordrecht: Kluwer)

Leka K. D., L. Mickey D., Uitenbroek H., Wagner E. L., Metcalf T. R., 2012, *Solar Phys*, 278, 471

Lites, B. W., Akin, D. L., Card, G., et al. 2013, *Sol. Phys.*, 283, 579

Ramelli R. , Balemi S., Bianda M., Defilippis I., Gamma L., Hagenbuch S., Rogantini M., Steiner P., Stenflo J. O., 2010, "ZIMPOL-3: a powerful solar polarimeter", SPIE conference proceedings, SPIE conference on Astronomical Telescopes + Instrumentation in San Diego, USA, 27 June - 2 July 2010, 7735, 77351Y, doi: 10.1117/12.857120

Rayrole J., 1967, *Annales d'Astrophysique*, 30, 257.

Sahal-Br echot S., Malinovsky M., Bommier V., 1986, *A&A*, 168, 284

Semel M., 1967, *Annales d'Astrophysique*, 30, 513

Socas-Navarro H., Trujillo Bueno J., Ruiz Cobo B., 2000, *ApJ*, 530, Issue 2, pp. 977-993

Stenflo J. O., 1982, *Sol. Phys.*, 80, 209

Stenflo J.O., 1994, *Solar Magnetic Fields* (Dordrecht: Kluwer)

Trujillo Bueno J., Shchukina N., Asensio Ramos A., 2004, *Nature*, 430, 326

Tsuneta, S., Ichimoto, K., Katsukawa, Y., et al. 2008, *Sol. Phys.*, 249, 167

Uitenbroek H., 2001, *ApJ*, 557, 389

Uitenbroek H., 2003, *ApJ*, 592, 1225.

Uitenbroek H., 2011, In: Kuhn, J.R., Harrington, D.M., Lin, H., Berdyugina, S.V., Trujillo-Bueno, J., Keil, S.L., Rimmele, T. (eds.) CS-437, *Astron. Soc. Pac.*, San Francisco, 439.